Splitting of neutral mechanical plane of conformal, multilayer piezoelectric mechanical energy harvester

Yewang Su, Shuang Li, Rui Li, and Canan Dagdeviren

Citation: Applied Physics Letters **107**, 041905 (2015); doi: 10.1063/1.4927677
View online: http://dx.doi.org/10.1063/1.4927677
View Table of Contents: http://scitation.aip.org/content/aip/journal/apl/107/4?ver=pdfcov
Published by the AIP Publishing

Splitting of neutral mechanical plane of conformal, multilayer piezoelectric mechanical energy harvester

Yewang Su,[1,2,a)] Shuang Li,[1] Rui Li,[3] and Canan Dagdeviren[4,5,a)]
[1]*State Key Laboratory of Nonlinear Mechanics, Institute of Mechanics, Chinese Academy of Sciences, Beijing 100190, China*
[2]*Department of Civil and Environmental Engineering, Northwestern University, Evanston, Illinois 60208, USA*
[3]*State Key Laboratory of Structural Analysis for Industrial Equipment, Department of Engineering Mechanics, Dalian University of Technology, Dalian 116024, China*
[4]*The David H. Koch Institute for Integrative Cancer Research, Massachusetts Institute of Technology, Cambridge, Massachusetts 02139, USA*
[5]*Department of Materials Science and Engineering, Beckman Institute for Advanced Science and Technology, and Frederick Seitz Materials Research Laboratory, University of Illinois at Urbana-Champaign, Urbana, Illinois 61801, USA*

(Received 2 May 2015; accepted 20 July 2015; published online 29 July 2015)

Flexible piezoelectric mechanical energy harvesters (MEHs) are of recent interest as an important emerging variant of traditional piezoelectric devices. The design of stacking multilayer MEHs with adhesive in between is an effective way to enhance the magnitude of power generation. Here, we present an analytic model to study the mechanical behavior of the multilayer MEHs based on lead zirconate titanate (PZT) subjected to Euler buckling. Being different from the hypothesis of the plane section for the entire stack, it is found that each polyimide (PI) layer holds plane section of its own, while soft adhesives serve as shear lags. Accordingly, the neutral mechanical plane is split into multiple ones. The deformation is almost the same for each PI layer, as well as PZT arrays, which is very beneficial to avoid the premature failure of devices. The extreme cases and the transition of these cases are all captured quantitatively with a unified analytic model which is verified by the finite element method. A dimensionless parameter is obtained to characterize the degree of the splitting of neutral mechanical plane, which is significant for the design of the multilayer PZT MEHs. © *2015 AIP Publishing LLC*. [http://dx.doi.org/10.1063/1.4927677]

Piezoelectric devices have been under rapid development in recent years and they provide many important potential applications such as piezoelectric mechanical energy harvesters (MEHs). As researchers continue looking for new sources of energy for sustainable future, piezoelectric materials, such as ZnO,[1] lead zirconate titanate (PZT),[2,3] and Poly(vinylidenefluoride) (PVDF),[4] emerge as prospective solutions that can produce electrical energy from mechanical motion of natural body processes (e.g., walking and breathing) via their ability to convert mechanical motions to electric power.[5] PZT based nanogenerators are being investigated because they can generate much higher power and voltage outputs than other semiconductive nanomaterials, and can offer high efficiency (~80%) in mechanical to electrical energy conversion.[6] PZT has excellent piezoelectric property; however, it has a disadvantage due to its brittleness as a ceramic material and its strain limitation (<1%).[7] To overcome this limitation, devices built with PZT, including other brittle piezoelectric materials, were typically integrated with stretchable substrates, as demonstrated by several research groups.[8,9] For instance, the integration of piezoelectric PZT ribbons onto flexible rubber substrate (e.g., Polydimethylsiloxane (PDMS)) offers an efficient and flexible energy conversion that creates a new opportunity for future energy harvesting systems.[8,10] Recently, a co-integrated collection of such energy harvesting elements in multilayer configuration with rectifiers and microbatteries provided an entire flexible system. The system is capable of viable integration with the beating heart via medical sutures and operation with a high peak voltage of 8.1 V and efficiency of ~2%.[3]

The magnitude of power generation to power bio-medical devices is an important aspect. It can be enhanced by stacking multiple PZT MEHs, as demonstrated in Fig. 1(a). Bending test shown in Fig. 1(b) reveals that peak voltage could be increased from 3.7 V (single PZT MEH) to 5.8 V and 8.1 V by stacking 3 and 5 PZT MEHs,[3] respectively. The mechanical behavior of the multilayer PZT MEHs is rather complex due to the coupling deformation among the polyimide (PI) layers and silicone layers, which serve as the substrates of PZT arrays and adhesive layers, respectively. From the view point of mechanical strength, the ideal design is that all the PZT MEHs reach their respective failure strength simultaneously, so that the failure strength of the entire stack is exactly that of a single MEH. Improper design may induce premature failure of the devices. Here, the mechanical behavior of multilayer PZT MEHs is studied via both a quantitative analytic model and the finite element method (FEM).

Figure 1(c) shows a model for a stack of length L consisting of three PI layers with thickness t_{PI} and two silicone layers with thickness $t_{silicone}$ in between. The influence of the attached PZT arrays on the PI layers is neglected so that the analysis is focused on the essence of the problem. Euler buckling dominates the deformation mode of the stack that is subject to compression ΔL. The mechanical behavior of a single-layer PI has been well studied by Song *et al.*,[11] as

[a)]Authors to whom correspondence should be addressed. Electronic addresses: yewangsu@imech.ac.cn and canand@mit.edu

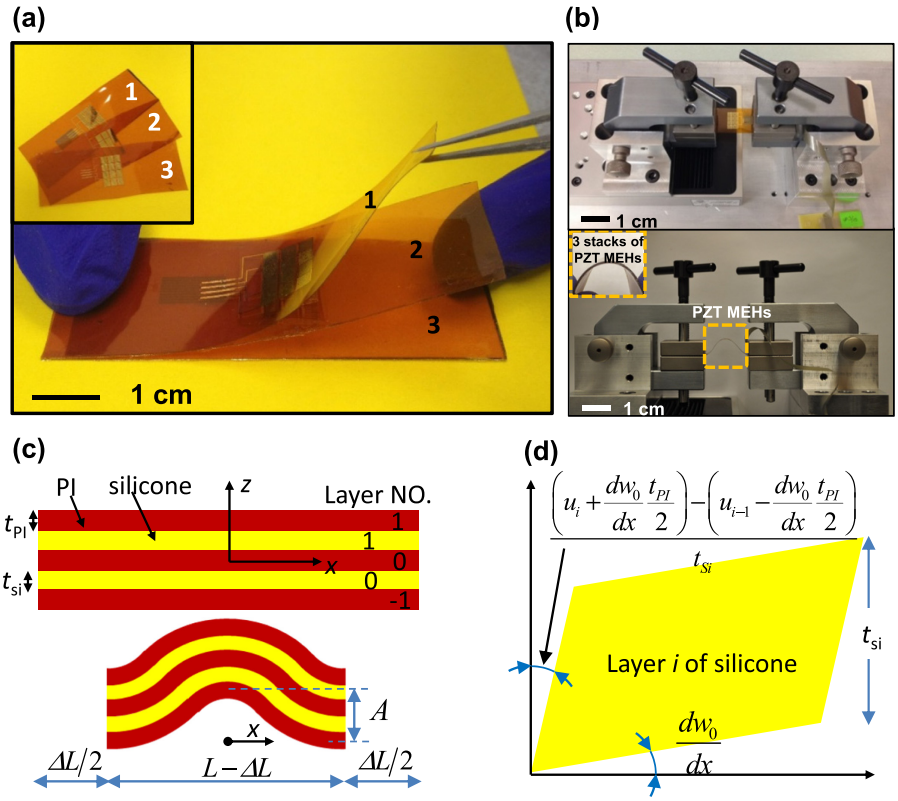

FIG. 1. (a) Stacking and (b) bending test of three PZT MEHs. (c) Theoretical model for a stack of three PZT MEHs. (d) Shear strain of a silicone layer.

well as by Su *et al.*[12] in the systematic theory of buckling. The vertical and horizontal displacements are obtained as

$$\begin{cases} w_0 = \dfrac{A}{2}\left(1+\cos\dfrac{2\pi x}{L}\right) \\ u_0 = \dfrac{\pi A^2}{16L}\sin\dfrac{4\pi x}{L} - \dfrac{\Delta L}{L}x, \end{cases} \tag{1}$$

where $A = (2L/\pi)\sqrt{\varepsilon_{applied} - \varepsilon_0}$ is the amplitude, $\varepsilon_{applied} = \Delta L/L$ and $\varepsilon_0 = \pi^2 t_{PI}^2/(3L^2)$ are the applied strain and membrane strain, respectively. The membrane strain ε_0 is much smaller than the applied strain $\varepsilon_{applied}$, and can be neglected for simplification. Therefore, $A = (2L/\pi)\sqrt{\varepsilon_{applied}}$ will be used in the following derivation. The assumption of plane section is usually used for the bending of the multiplayer stacks. However, the assumption is only applicable to the stacks with similar Young's moduli.[13] Here, the assumption is relaxed so that each PI layer holds plane section of its own and the adhesive (silicone) layers serve as shear lags transferring shear stresses between PI layers[14] because adhesive layers are relatively thin and soft. Being inspired by the analysis of a single layer PI, it is reasonable to assume that the vertical displacement for a single-layer PI holds for the PI layers in the multilayer stack while the difference appears in the horizontal displacement and membrane strain due to the shear effect of soft silicone. Let

$$u_i = u_0 + \Delta u_i, \tag{2}$$

be the horizontal displacement of the central axis of PI layer i, where Δu_i is the displacement increment with respect to that of a single layer, $i\ (=-1, 0, 1)$ denotes the number of PI in the stack as shown in Fig. 1(c). The symmetric condition and the boundary condition for the displacement increment are

$$\Delta u_i(x=0) = \Delta u_i(x=L/2) = 0, \tag{3}$$

since u_0 meets the boundary condition $u_0(x=L/2) = -\Delta L/2$. According to the analysis by Song *et al.*,[11] the membrane strain of a single-layer PI without soft adhesives is $\varepsilon_0 = \pi^2 t_{PI}^2/(3L^2)$, which is quite small and can be neglected. (The correctness is also confirmed by the final agreement of the finite element results and the analytic calculation based on this assumption.) Therefore, the membrane strain and its increment with respect to that of a single-layer PI become

$$\varepsilon_{m,i} = \Delta\varepsilon_{m,i} = \frac{\partial \Delta u_i}{\partial x}. \tag{4}$$

On the other hand, the shear strain of a silicone layer, as shown in Fig. 1(d), consists of both the horizontal mismatch of adjacent PI layers and the gradient of the vertical displacement,[14] which gives

$$\begin{aligned} \gamma_{si,i} &= \frac{\left(u_i + \dfrac{dw_0}{dx}\dfrac{t_{PI}}{2}\right) - \left(u_{i-1} - \dfrac{dw_0}{dx}\dfrac{t_{PI}}{2}\right)}{t_{si}} + \frac{dw_0}{dx} \\ &= \frac{\Delta u_i - \Delta u_{i-1}}{t_{Si}} + \left(1 + \frac{t_{PI}}{t_{Si}}\right)\frac{dw_0}{dx}. \end{aligned} \tag{5}$$

With a given applied compression ΔL, the total elastic energy of the whole system consists of the membrane energy and bending energy of PI layers and shear energy of silicone layers

$$U = \sum_{i=-1}^{1} \int_0^{L/2} \left[\frac{1}{2} \frac{E_{PI} t_{PI}}{1-\nu_{PI}^2} \varepsilon_{m,i}^2 + \frac{1}{24} \frac{E_{PI} t_{PI}^3}{1-\nu_{PI}^2} \left(\frac{d^2 w_0}{dx^2} \right)^2 \right] dx + \frac{1}{2} \frac{E_{si} t_{si}}{2(1+\nu_{si})} \sum_{i=0}^{1} \int_0^{L/2} \gamma_{si,i}^2 dx, \quad (6)$$

where E_{PI} and E_{si} are the Young's moduli, and ν_{PI} and ν_{si} are the Poisson's ratios of PI and silicone, respectively. Variation of the total elastic energy of the whole system, together with Eq. (3), gives the governing equations

$$\begin{cases} \dfrac{\partial^2 \Delta u_1}{\partial x^2} - \dfrac{\alpha\beta}{2t_{si}} \left[\dfrac{\Delta u_1 - \Delta u_0}{t_{Si}} + \left(1 + \dfrac{1}{\beta}\right) \dfrac{dw_0}{dx} \right] = 0 \\ \dfrac{\partial^2 \Delta u_0}{\partial x^2} + \dfrac{\alpha\beta}{2t_{si}} \left[\dfrac{\Delta u_1 + \Delta u_{-1} - 2\Delta u_0}{t_{Si}} \right] = 0 \\ \dfrac{\partial^2 \Delta u_{-1}}{\partial x^2} + \dfrac{\alpha\beta}{2t_{si}} \left[\dfrac{\Delta u_0 - \Delta u_{-1}}{t_{Si}} + \left(1 + \dfrac{1}{\beta}\right) \dfrac{dw_0}{dx} \right] = 0, \end{cases} \quad (7)$$

where $\alpha = [E_{si}(1-\nu_{PI}^2)]/[E_{PI}(1+\nu_{si})]$ is a dimensionless constant that scales with the Young's modulus ratio and $\beta = t_{si}/t_{PI}$ is the thickness ratio. The differential equation system (7), together with the vertical displacement Eq. (1) and the boundary condition Eq. (3), gives the solution for the displacement increments as

$$\Delta u_0 = 0,\ \Delta u_1 = -\Delta u_{-1} = \frac{2L\alpha\gamma(1+\beta)\sqrt{\varepsilon_{applied}}}{\alpha\gamma^2 + 8\pi^2\beta} \sin\left(\frac{2\pi x}{L}\right), \quad (8)$$

where $\gamma = L/t_{PI}$ is the aspect ratio of the PI layer. According to the geometrical relation in Eq. (4), the membrane strain of each layer is obtained as

$$\varepsilon_{m,0} = 0,\ \varepsilon_{m,1} = -\varepsilon_{m,-1} = \frac{4\pi\alpha\gamma(1+\beta)\sqrt{\varepsilon_{applied}}}{\alpha\gamma^2 + 8\pi^2\beta} \cos\left(\frac{2\pi x}{L}\right). \quad (9)$$

PZT arrays are located at the surface center (x = 0) of each PI layer. The strain at this location is of importance. The maximum bending strain at the center is

$$\varepsilon_{\text{bending,max}}|_{x=0} = -\frac{t_{PI}}{2} \frac{d^2 w_0}{dx^2}\bigg|_{x=0} = \frac{2\pi\sqrt{\varepsilon_{applied}}}{\gamma}, \quad (10)$$

which is the same for all the PI layers. The membrane strain is different for each PI layer according to the results in Eq. (9). Define

$$\eta = \frac{\Delta\varepsilon_{m,1}}{\varepsilon_{\text{bending,max}}}\bigg|_{x=0} = \frac{2\alpha\gamma^2(1+\beta)}{\alpha\gamma^2 + 8\pi^2\beta}, \quad (11)$$

as the ratio of the membrane strain to the maximum bending strain at the center. It represents how different the strain is among these PI layers. Figure 2 shows the trend of η with the change of α and β. Soft (small α) and thick (big β) adhesive gives small η, for instance, $\eta = 0.296$ for $\alpha = 0.0000142$ and $\beta = 0.133$ in the experiment design ($E_{PI} = 2.5$ GPa, $\nu_{PI} = 0.34$, and $t_{PI} = 75\ \mu$m, for PI; $E_{si} = 60$ kPa, $\nu_{si} = 0.49$, and $t_{si} = 10\ \mu$m, for silicone; $L = 2.5$ cm), which means that the membrane strains of the top and bottom PI layers are small, and the strain distribution is almost the same (see Figure 3(a)) for each PI layer. In this case, plane section holds for each PI layer, and multiple neutral mechanical planes exist in the stack, which is called splitting of neutral mechanical plane.[13] Equation (11) incorporates the extreme cases: (1) $\eta = 0$ for $E_{si} = \alpha = 0$, in which all the membrane strains are zero and each PI layer deforms as a single layer, and the neutral mechanical plane is split into multiple ones; (2) $\eta = 2$ for $t_{si} = \beta = 0$, in which the plane section holds for the whole stack of the three PI layers with thickness $3t_{\text{PI}}$, where only one neutral mechanical plane exists; (3) $\eta = 2(1+\beta)$ for $E_{si} = \infty$ and $\alpha = \infty$, in which the plane section holds for the whole stack of the three PI layers together with the two adhesive layers with thickness $(3t_{\text{PI}} + 2t_{\text{si}})$, where only one neutral mechanical plane exists. The other extreme case is that $t_{si} = \infty$ and $\beta = \infty$. However, the present analytic model is based on the assumption that the adhesive layer is relatively thin (and soft). Otherwise, the assumption of shear lag for the adhesive layers does not hold. Therefore, the resulting equations are not valid for this extreme case. Besides these extreme cases, the transition regimes can be captured by η as well, which will be shown in the next paragraph and Fig. 3. The dimensionless parameter η in terms of the materials and

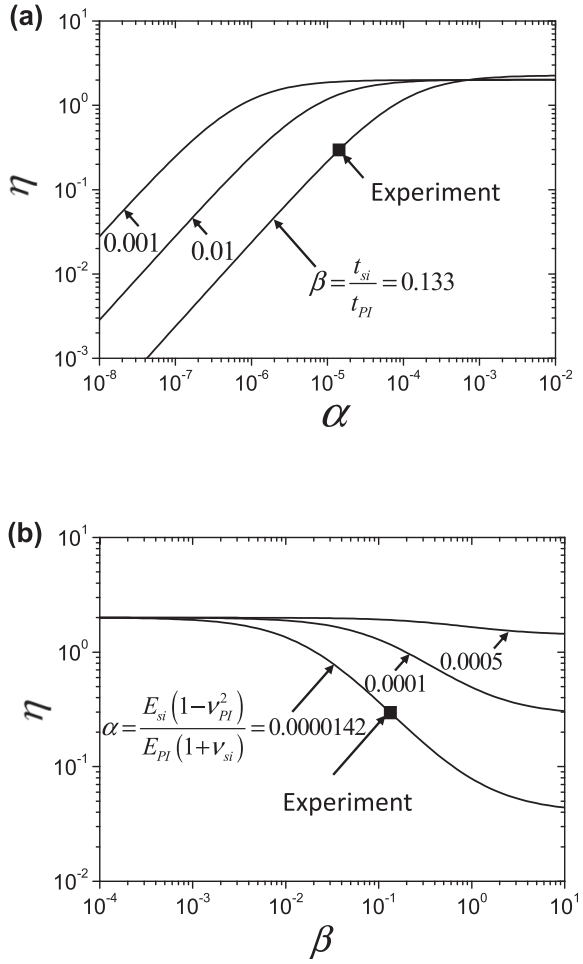

FIG. 2. Ratio of membrane strain to bending strain versus (a) the dimensionless constant α and (b) the thickness ratio β.

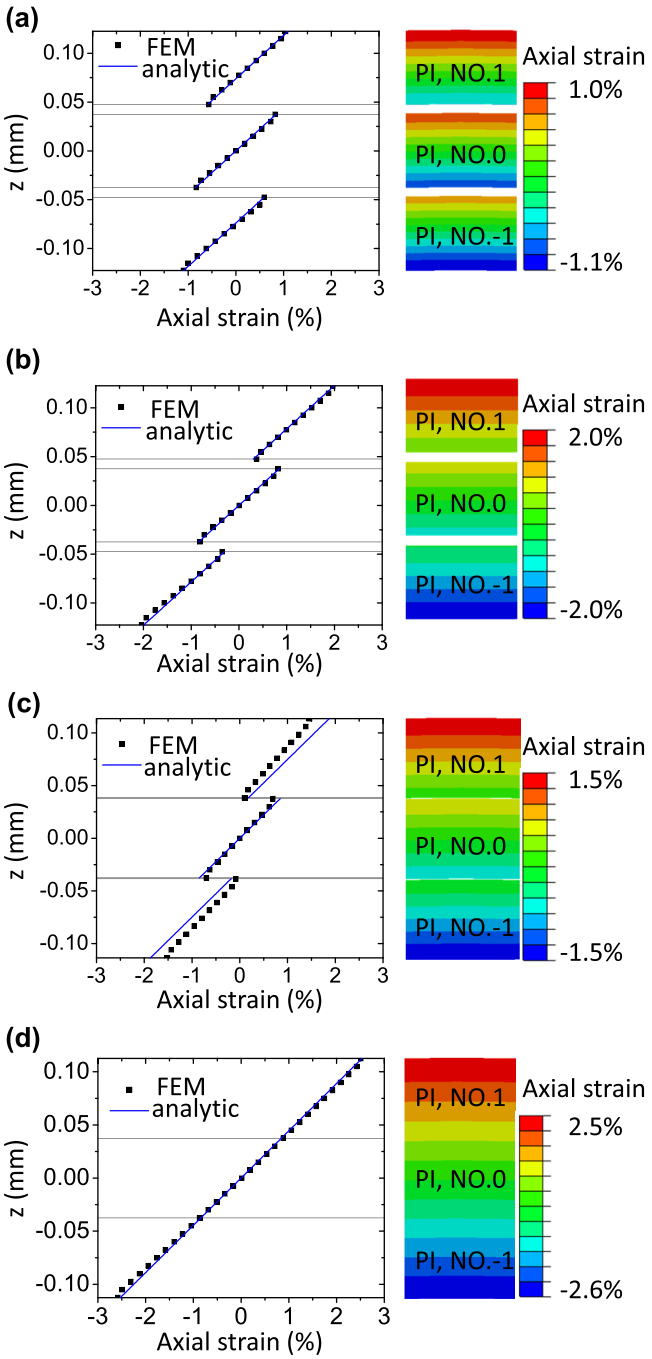

FIG. 3. Comparison of axial strain distributions ($\Delta L = 5$ mm) between analytic model and FEM for (a) the experimental design ($\eta = 0.296$, $E_{si} = 60$ kPa, $t_{si} = 10\,\mu$m), designs with (b) harder adhesives ($\eta = 1.36$, $E_{si} = 600$ kPa, $t_{si} = 10\,\mu$m), (c) thinner adhesives ($\eta = 1.21$, $E_{si} = 60$ kPa, $t_{si} = 1\,\mu$m), and (d) adhesives of zero thickness ($\eta = 0$, $t_{si} = 0$), respectively.

geometry properties clearly characterizes the degree of splitting of the neutral mechanical plane for the multilayer stack.

The axial strain of each PI layer consists of both bending strain and membrane strain. For each layer of PI, the bending strain is the same as $\varepsilon_{bending,i}|_{x=0} = [z - i(t_{PI} + t_{Si})] / [t_{PI}/2]\varepsilon_{\text{bending,max}}|_{x=0}$, where i denotes the layer number and $z - i(t_{PI} + t_{Si})$ is the distance from the current location to the central axis of the ith PI layer (Fig. 1(c)). On the other hand, extension of Eq. (11) gives the membrane strain for the ith PI layer as $\Delta\varepsilon_{m,1}|_{x=0} = i\eta\,\varepsilon_{\text{bending,max}}|_{x=0}$. These derivations, together with Eq. (10), yield the distribution of the axial strain at $x = 0$ as

$$\varepsilon_i|_{x=0} = \left[\frac{z - i(t_{PI} + t_{Si})}{t_{PI}/2} + i\eta\right]\frac{2\pi\sqrt{\varepsilon_{applied}}}{\gamma}, \qquad (12)$$

where the vertical coordinate z starts from the center of middle PI layer.

Finite element analysis by ABAQUS software package[15] is used to validate the analytic results of Eq. (12) in the main text. Plane strain models are established with the sizes which are the same as those in the analytic model. Four-node bilinear plane strain element CPE4R is adopted for both PI layers and adhesive layers, without any assumption of plane section or shear lag. Symmetric boundary condition is imposed and only the right half model with length $L/2$ is analyzed. Axial compression is applied by displacement loading $\Delta L/2 = 2.5$ mm on the right edge. In order to yield the buckling model, small perturbation along the vertical direction is applied. The strain distribution along the axial direction is extracted for comparison with the analytic results.

As shown in Fig. 3, the prediction by Eq. (12) agrees well with the FEM for both the extreme cases as discussed above (Figs. 3(a) and 3(d)) and the transition cases (Figs. 3(b) and 3(c)). For the design of the experiment, Fig. 3(a) shows that the adhesive is soft and thick enough so that the strain distribution on each PI layer is almost the same. No premature failure occurs on the top and bottom devices. Figures 3(b) and 3(c) show that the analytic model is capable of predicting the transition regimes with harder and thinner adhesive layers. Figure 3(d) verifies the extreme case of zero thickness of adhesive layers. In the experiment,[3] the stacks of both three layers and five layers are adopted. The solution of the stack of five layers can be obtained with the same approach but more equations. It is verified by FEM that the five PI layers deform separately with very little interaction when the thickness and Young's modulus are the same as in the three layers stacked PI, as shown in Fig. 4.

Smaller value of η implies a greater degree of splitting of the neutral mechanical plane and more similar distribution of the strain for each PI layer. From this point of view, softer

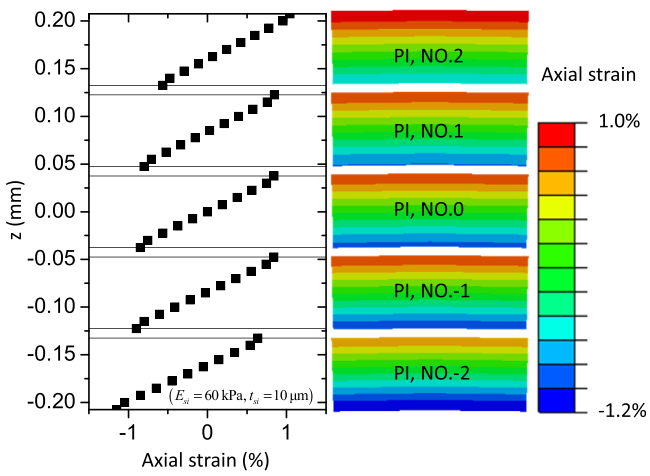

FIG. 4. Axial strain distribution for a stack of five PI layers.

and thicker adhesive layer is more beneficial to avoid the premature failure of devices. One extreme case is the empty gap instead of any adhesives. However, the other function of the adhesive is bonding the devices together to avoid physical separation. Therefore, the quantitative analysis of the splitting of the neutral mechanical plane is necessary and significant.

In summary, the mechanical behavior of the stack design for piezoelectric energy harvester is studied by an analytic model and verified by FEM. The ratio of the membrane strain to the bending strain at the center is obtained analytically to characterize the strain distribution of PI layers and the degree of the splitting of neutral mechanical plane. Soft and thick adhesive reduces the interaction among PI layers and is helpful for the splitting of the neutral mechanical plane and avoiding the premature failure of the whole devices.

This work was supported by the National Natural Science Foundation of China (Grant 11302038) and China Postdoctoral Science Foundation (2014T70243). We thank Professor John A. Rogers of the University of Illinois for his helpful discussion and continued support. C.D. thanks P. Joe for her assistance on experimental part.

[1]C. Dagdeviren, S. W. Hwang, Y. Su, S. Kim, H. Cheng, O. Gur, R. Haney, F. G. Omenetto, Y. Huang, and J. A. Rogers, Small **9**(20), 3398 (2013).
[2]C. Dagdeviren, Y. Su, P. Joe, R. Yona, Y. Liu, Y.-S. Kim, Y. Huang, A. R. Damadoran, J. Xia, L. W. Martin, Y. Huang, and J. A. Rogers, Nat. Commun. **5**, 4496 (2014).
[3]C. Dagdeviren, B. D. Yang, Y. Su, P. L. Tran, P. Joe, E. Anderson, J. Xia, V. Doraiswamy, B. Dehdashti, and X. Feng, Proc. Natl. Acad. Sci. U. S. A. **111**(5), 1927 (2014).
[4]L. Persano, C. Dagdeviren, Y. Su, Y. Zhang, S. Girardo, D. Pisignano, Y. Huang, and J. A. Rogers, Nat. Commun. **4**, 1633 (2013).
[5]T. Starner, IBM Syst. J. **35**(3.**4**), 618 (1996).
[6]A. M. Flynn and S. R. Sanders, IEEE Trans. Power Electron. **17**(1), 8 (2002).
[7]T. Tanimoto, K. Okazaki, and K. Yamamoto, Jpn. J. Appl. Phys., Part 1 **32**(9S), 4233 (1993).
[8]X. Feng, B. D. Yang, Y. Liu, Y. Wang, C. Dagdeviren, Z. Liu, A. Carlson, J. Li, Y. Huang, and J. A. Rogers, ACS Nano **5**(4), 3326 (2011).
[9]E. M. Alkoy, C. Dagdeviren, and M. Papila, J. Am. Ceram. Soc. **92**(11), 2566 (2009); Yi. Qi, J. Kim, T. D. Nguyen, B. Lisko, P. K. Purohit, and M. C. McAlpine, Nano Lett. **11**(3), 1331 (2011).
[10]Yi. Qi, N. T. Jafferis, K. Lyons, Jr., C. M. Lee, H. Ahmad, and M. C. McAlpine, Nano Lett. **10**(2), 524 (2010).
[11]J. Song, Y. Huang, J. Xiao, S. Wang, K. C. Hwang, H. C. Ko, D.-H. Kim, M. P. Stoykovich, and J. A. Rogers, J. Appl. Phys. **105**(12) 123516 (2009).
[12]Y. Su, J. Wu, Z. Fan, K.-C. Hwang, J. Song, Y. Huang, and J. A. Rogers, J. Mech. Phys. Solids **60**(3), 487 (2012).
[13]L. Li, H. Lin, S. Qiao, Yi. Zou, S. Danto, K. Richardson, J. D. Musgraves, N. Lu, and J. Hu, Nat. Photonics **8**, 643 (2014); N. Lu, S. Yang, and S. Qiao, paper presented at the SPIE Defense+ Security, 2014.
[14]Y. Su, B. Ji, K.-C. Hwang, and Y. Huang, J. Mech. Phys. Solids **60**(10), 1771 (2012).
[15]ABAQUS 6.13 [Computer software], Pawtucket, RI, Dassault Systèmes.